Investigation of performance enhancement of a building integrated photovoltaic thermal system

Tingting Yang, Andreas K. Athienitis
Dept. of Building, Civil and Environmental Engineering, Concordia University, Montréal, Québec, Canada

Abstract

In this paper, a new design of a BIPV/T system with added glazed air collector section and wire mesh is studied for enhancing thermal performance. The vertical solar air collector is connected in series with the BIPV/T system to raise outlet air temperature in winter, and the wire mesh is placed in the channel behind the glazing of the solar air heater. A computer program is developed based on a mathematical model. Comparative analysis shows that the addition of wire mesh benefits efficiency at mass flow rates of less than 0.03 kg/s and that heat transfer enhancement depends on wire mesh geometry. The optimum mass flow rate of the wire mesh packed system is determined to be between 0.01kg/s to 0.03 kg/s; the efficiency is about 8.5% higher than that without the mesh, and outlet air temperature is typically increased by 4 °C to 11 °C.

1 Introduction

Photovoltaic (PV) modules absorb up to 95% of incident solar irradiation, while only 5-20% of the incident energy is typically converted into electricity and the remaining energy becomes heat. This effect can result in PV panels reaching temperatures as high as 35°C above ambient temperature on sunny days (van Helden et al., 2004). As PV modules get hotter, they become less efficient, which can cause substantial decline in electricity generation during hot sunny days. In the building sector, a promising solution to this issue are the building-integrated photovoltaic thermal (BIPV/T) systems. Efforts have been devoted to improve the performance of BIPV/T systems by simultaneously increasing electrical and thermal efficiencies at the same time by many researchers.

Shahsavar et al. (2011) described a BIPV/T system that cooled the photovoltaic panels by ventilation in winter and exhaust air in summer, and the ventilation heat gain in winter also compensated for part of the heating demand. Numerical results revealed that the cooling effect on the $10m^2$ PV panels resulted in 129.2 kWh extra electricity production in summer from April to September and 55.9 kWh extra in winter from October to March.

A full scale field study was carried out and a computational fluid dynamics model was set up by Corbin and Zhai (2010) to investigate the thermal and electrical performance of a BIPV/T system with active heat recovery by water-cooled absorber. Such a system is particularly recommended for lower latitudes where the circulating water temperature could be suitable for domestic hot water use. Thermal and combined thermal-electrical efficiencies of the system reached 19% and 34.9%, respectively.

Chow et al. (2003) examined four design options via the ESP-r program for a hotel building in Macau, a subtropical city in China. Their results showed that electricity production differed by less than 1% with or without the air gap between PV and building facade, which is naturally ventilated by wind-induced and buoyancy effects. However, the

addition of an air gap could reduce the space heat gain of the hotel by as much as 50% from May to October. Chow et al. (2007) tested the performance of two photovoltaic-thermosyphon water systems that made use of the flat box structure under subtropical climate. The comparative study showed that having the water entering the collector at the lower header is suitable for thermosyphon systems.

For a cold climate location in India, Agrawal and Tiwari (2010) carried out an analysis to select an appropriate BIPV/T system according to their energy and exergy performances, which is based on a one-dimensional transient model. Results showed that for a constant air mass flow rate and a constant air velocity, system connected in series and in parallel, respectively, gives a better performance.

Athienitis et al. (2011) developed a prototype BIPV/T system that was integrated with transpired collector. Such a prototype was tested in Montreal's cold climate. Assuming that electricity can be converted to four times as much heat, the equivalent thermal efficiency of the BIPV/T system is 7-17% higher than unglazed transpired collector covering the same area. The concept of this prototype served as the basis for the JMSB (John Molson School of Business) building demonstration project in Montreal, in which 384 building-integrated PV modules cover 70% of the unglazed transpired collector area. This system generates up to 25kW electricity and 75kW heat of ventilation fresh air preheating, and peak combined solar energy utilization efficiency of 55% has been achieved.

Chen et al. (2010) designed a BIPV/T system that was thermally coupled with a ventilated concrete slab for a prefabricated, two-storey detached, low energy solar house located in Eastman, Quebec, and the BIPV/T system performance was later analyzed with monitored data, which indicated that its typical thermal efficiency of the BIPV/T system was 20%.

The thermal enhancement with wire mesh in solar air heaters attracted many researchers in the past decade. Thakur et al. (2003) carried out experiments on low-porosity wire mesh and developed correlations for heat transfer coefficient and friction factor. Prasad et al. (2009) carried out experimental tests to find out the heat transfer and friction characteristics of packed bed solar air heater using wire mesh as packing material. Compared to a conventional solar air heater, the efficiency enhancement provided by wire mesh was between 76.9% and 89.5%. The performance of single and double pass solar air heaters with wire mesh packed bed was experimentally studied by Aldabbagh et al. (2010). The thermal efficiency of a packed bed was substantially enhanced compared to that of a conventional collector — the maximum efficiencies for the single and double pass air collectors were 45.93% and 83.65% respectively. Another experiment was carried out by Omojaro et al. (2010) by adding fins to the single and double pass solar air heater packed by wire mesh; the maximum thermal efficiencies were further enhanced to 59.62% and 63.74% respectively.

The energy performance of a house with three configurations of open loop air-based BIPV/T systems was modelled by Pantic et al. (2010). It was found that with the addition of 1.5m vertical glazed solar air collector connected in series with the PV/T collector, significant increase in outlet air temperatures were achieved in winter. In this paper, an improvement to Pantic et al. (2010) design is proposed which adds packed wire mesh to the vertical glazed solar air collector. Mathematical models are implemented in a computer program and the performance is studied. The motivation for this work is that in cold climates such as most of Canada, the high levels of solar radiation on cold sunny days can be better utilized in open loop air systems connected to a solar source heat pump that can provide space and water heating.

Nomenclature

A	Heat transfer area between air and wire mesh, m²
A_f	Frontal area, m²
c_p	Specific heat of air, J/(kg·K)
D	Depth of the collector bed, m
D_h	Hydraulic diameter, m
d_w	Wire diameter of the wire matrices, m
dx	Length of a control volume element, m
f_p	Average friction factor for packed bed
f_c	Average friction factor for conventional duct
G_0	Relative mass flow rate for a packed bed (kg/m²·s)
h	Heat transfer coefficient, W/(m²·K)
J_h	Colburn J_h factor
k	Conductivity, W/(m·K)
L	Length of collector, thickness of EVA, m
$\dot{m}$	Mass flow rate of air, kg/s
n	Number of wire mesh layers
Nu	Nusselt number
P	Porosity of the wire mesh matrix
Pr	Prandtl number
p_t	Pitch of wire mesh, m
Re	Reynolds number
Re_p	Packed bed Reynolds number
r_h	Hydraulic radius for the packed bed, m
S	Solar irradiation, W/m²
St_p	Stanton number for packed bed
T	Temperature, K
u	Air velocity in the duct, m/s
V_{wind}	Wind velocity, m/s
W	Width of the collector, m

Greek letters

α	Absorptivity
β	Packing factor
ε	Surface emmisivity
τ	Transmissivity
μ	Dynamic viscosity of air, N·s/m²
ρ	Density of air, kg/m³
η	efficiency
σ	Stefan-Boltzman constant (= $5.67\times10^{-8}\ W/(m^2K^4)$)

Subscripts

a	Ambient air
b	Insulation
c	Convective heat transfer
e	EVA
f	Air flow
g	Glass of the PV module, glazing of the solar air heater
pv	Components in the PV covered portion of the system
PVF	Polyvinyl fluoride
r	Radiative heat transfer
s	Solar cell
sah	Solar air heater
sky	Sky radiation
w	Wire mesh
room	Room air

Acronym

BIPV/T	Building-integrated photovoltaic/thermal

2 Mathematical model

The open loop BIPV/T system is connected in series with a vertical solar air collector having packed wire mesh. As shown in Figure 1, air is further heated by the vertical solar air collector after flowing out of the BIPV/T channel, resulting in a higher outlet air temperature. For the case studied, the Kyocera KC200GT module is used, which measures 1.425 m long and 0.99 m wide, the depth of the channel is 0.04 m. The depth of the solar air heater was decided

based on the limiting value of optical depth as indicated in the work by Varshney L. & Saini S.J. (1998), which is 0.025 m. The length and width of the solar air heater is 1.0 m and 0.99m. The following assumptions have been applied to the system model:

- The system is in quasi steady state
- The transmittance of the EVA is 100%
- Temperature difference is neglected in the thickness direction for each component

The cross-section view of the BIPV/T part of the system is shown in Figure 2(a). The solar cells are encapsulated between two layers of EVA. EVA stands for ethylene vinyl acetate, and is used to surround and provide shock-absorbing protection to the the silicon cells. The upper EVA layer is protected by high-transmissivity glass, and the lower EVA is backed by PVF back sheet. PVF, also known as polyvinyl fluoride, offers moisture barrier, weathering resistance and electrical insulation functions to the PV module.

The BIPV/T channel is divided into 10 control volumes; the energy balance equations for a typical control volume are given below. Figure 3 shows a typical control volume and all the temperature nodes.

Glass:

$$\alpha_{pv,g} S_{pv} + \frac{T_{pv,s} - T_{pv,g}}{\frac{L_{pv,e}}{k_{pv,e}}} = h_{pv,a}\left(T_{pv,g} - T_{pv,a}\right) + h_{pv,rgs}\left(T_{pv,g} - T_{pv,sky}\right) \tag{1}$$

Solar cell:

$$\tau_{pv,g}\alpha_{pv,s} S_{pv} W dx = P_{electricity} + \frac{T_{pv,s} - T_{pv,g}}{\frac{L_{pv,e}}{k_{pv,e}}} W dx + \frac{T_{pv,s} - T_{pv,PVF}}{\frac{L_{pv,e}}{k_{pv,e}}} W dx \tag{2}$$

PVF back sheet:

$$\tau_{pv,g}\alpha_{pv,PVF}\left(1-\beta_{pv}\right) S_{pv} + \frac{T_{pv,s} - T_{pv,PVF}}{\frac{L_{pv,e}}{k_{pv,e}}} = h_{pv,cPVFf}\left(T_{pv,PVF} - T_{pv,f}\right) + h_{pv,rPVFb}\left(T_{pv,PVF} - T_{pv,b}\right) \tag{3}$$

Air:

$$\dot{m} c_p \Delta T_{pv,f} = h_{pv,cPVFf}\left(T_{pv,PVF} - T_{pv,f}\right) W dx + h_{pv,cbf}\left(T_{pv,b} - T_{pv,f}\right) W dx \tag{4}$$

Back insulation:

$$h_{pv,rPVFb}\left(T_{pv,PVF} - T_{pv,b}\right) = h_{pv,cbf}\left(T_{pv,b} - T_{pv,f}\right) + U_{pv}\left(T_{pv,b} - T_{pv,room}\right) \tag{5}$$

The cross-section view of the vertical solar air heater packed with wire mesh is shown in Figure 2(b). The energy balance equations are as follows:

Glazing:

$$\alpha_g S + h_{rwg}\left(T_w - T_g\right) = h_a\left(T_g - T_a\right) + h_{rgs}\left(T_g - T_{sky}\right) + h_{cgf}\left(T_g - T_f\right) \tag{6}$$

Wire mesh:

$$\tau_g \alpha_w S \cdot W dx = h_{rwg}\left(T_w - T_g\right) \cdot W dx + h_{cwf}\left(T_w - T_f\right) \cdot \frac{A}{10} + h_{rwb}\left(T_w - T_b\right) \cdot W dx \tag{7}$$

Air:

$$\dot{m} c_p \Delta T = h_{cgf}(T_g - T_f) W dx + h_{cbf}(T_b - T_f) W dx + h_{cwf}(T_w - T_f)\frac{A}{10} \quad (8)$$

Insulation:

$$h_{rwb}(T_w - T_b) = h_{cbf}(T_b - T_f) + U(T_b - T_{room}) \quad (9)$$

Heat transfer coefficient

Radiative heat transfer coefficient between a surface and the sky is shown in Eq. (10) (Eicker, 2003)

$$h_{rgs} = \sigma \varepsilon_g (T_g^2 + T_{sky}^2)(T_g + T_{sky}) \quad (10)$$

The sky temperature in Eq. (10) is given by the modified Swinbank equation of Fuentes (1987) as below:

$$T_{sky} = 0.037536 T_a^{1.5} + 0.32 T_a \quad (11)$$

The forced convective heat transfer between a surface and the wind is calculated using the correlation by Watmuff et al. (1977), as shown in Eq. (12)

$$h_a = 2.8 + 3.0 V_{wind} \quad (12)$$

For each control volume element, the radiative heat transfer coefficient between two parallel planes is given by Eq. (13)

$$h_{rgb} = \frac{\sigma (T_g^2 + T_b^2)(T_g + T_b)}{\frac{1}{\varepsilon_g} + \frac{1}{\varepsilon_b} - 1} \quad (13)$$

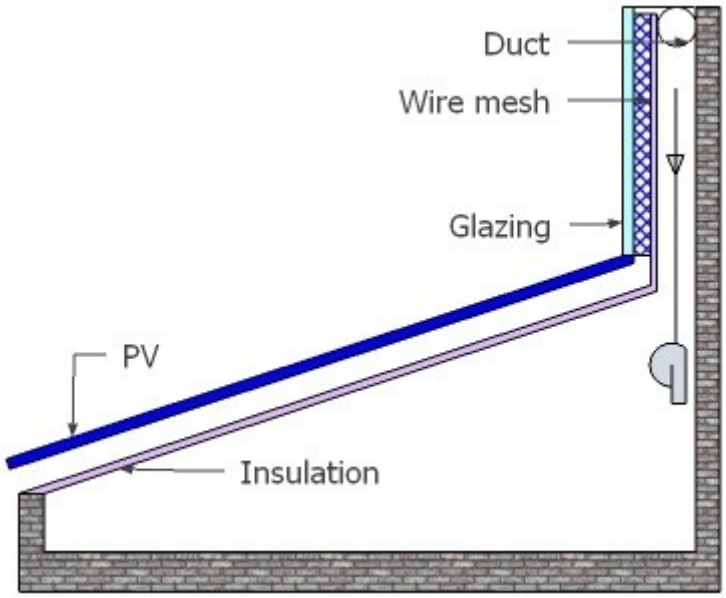

Figure 1: Schematic of the combination of BIPV/T system and solar air heater

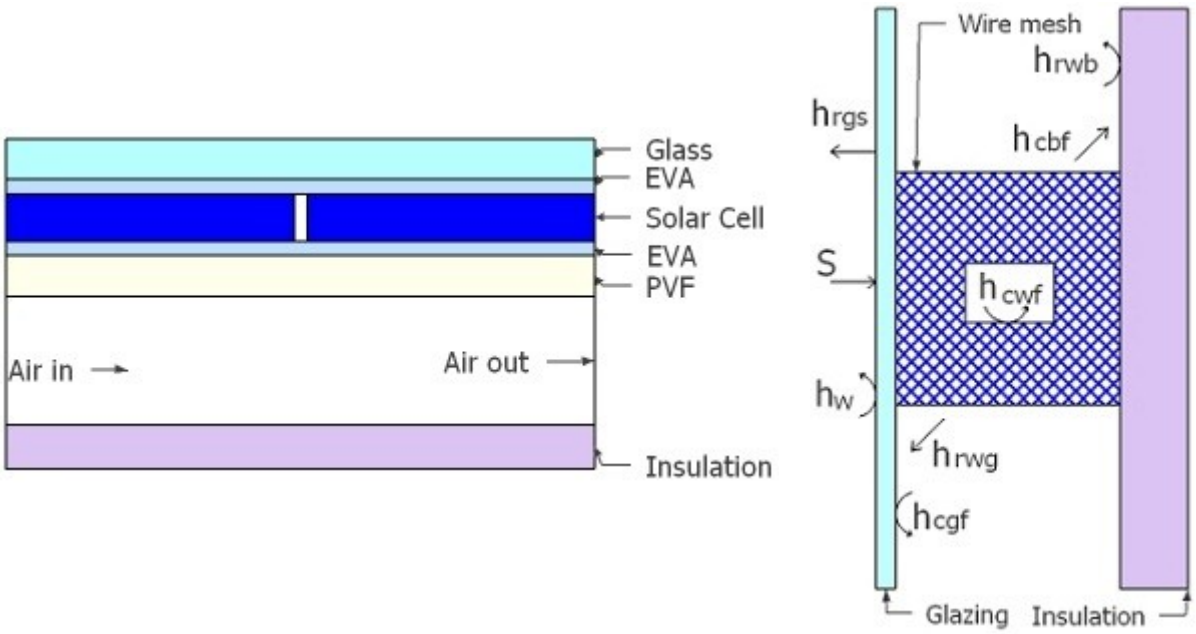

Figure 2: (a) Cross-section view of the BIPV/T system (b) Cross-section view of the wire mesh packed solar air heater

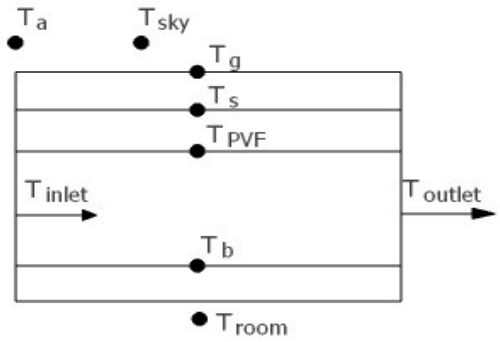

Figure 3: A typical control volume and all temperature nodes

Candanedo et al. (2011) studied the convective heat transfer coefficients in a BIPV/T system and correlated the Nusselt number for the top and bottom surfaces of the BIPV/T channel, which is utilized in this study.

For the top surface

$$Nu_{top} = 0.052\, Re^{0.78}\, Pr^{0.4} \qquad (250 \leqslant Re \leqslant 7500) \tag{14}$$

For the bottom surface

$$Nu_{bottom} = 1.017\, Re^{0.471}\, Pr^{0.4} \qquad (800 \leqslant Re \leqslant 7100) \tag{15}$$

The calculation of the convective heat transfer coefficient between wire mesh and air is based on the experimental investigation of Prasad et al. (2009).

To calculate the heat transfer coefficient, some geometrical parameters are needed. They are presented below.

The porosity of the wire screen matrix is determined by Eq. (16)

$$P = 1 - \frac{\pi n d_w^2}{2 p_t D}\left(1 + \frac{d_w^2}{p_t^2}\right)^{1/2} \tag{16}$$

The effective heat transfer area between the wire mesh and air is determined as

$$A = \frac{4 A_f L(1-P)}{d_w} \tag{17}$$

The hydraulic radius for the packed bed duct is given by Eq. (18)

$$r_h = \frac{P d_w}{4(1-P)} \tag{18}$$

The Colburn factor is expressed by Eq. (19)

$$J_h = 0.2563\left(\frac{1}{nP}\right)^{0.609}\left(\frac{P_t}{d_w}\right)^{0.7954} Re_p^{-0.63} \tag{19}$$

The relation between heat transfer coefficient, Colburn factor and Stanton number is evaluated by Eq. (20) and Eq. (21).

$$St_p = \frac{h}{G_0 c_p} \tag{20}$$

$$J_h = St_p Pr^{2/3} \tag{21}$$

In Eq. (20), the relative mass flow rate for a packed bed G_0 is given by Eq. (22)

$$G_0 = \frac{\dot{m}}{A_f P} \tag{22}$$

In the vertical solar air heater, the convective coefficient between plate and air flow is decided by Eq. (23) – (25).

$$h_c = \frac{k_{air}}{D_h}\left(1.86 \cdot \left(\frac{RePrD_h}{L}\right)^{1/3} \cdot \left(\frac{\mu}{\mu_s}\right)^{0.14}\right) \qquad Re < 2300 \tag{23}$$

$$h_c = \frac{k_{air}}{D_h}\left(0.116 \cdot (Re^{2/3} - 125) \cdot Pr^{1/3} \cdot \left(1 + \left(\frac{D_h}{L}\right)^{2/3}\right) \cdot \left(\frac{\mu}{\mu_s}\right)^{0.14}\right) \qquad 2300 < Re < 6000 \tag{24}$$

$$h_c = \frac{k_{air}}{D_h}\left(\frac{\left(\frac{f}{8} \cdot (Re - 1000) \cdot Pr\right)}{1 + 12.7 \cdot \sqrt{\frac{f}{8}} \cdot (Pr^{2/3} - 1)}\right) \cdot \left(1 + \left(\frac{D_h}{L}\right)^{2/3}\right) \qquad 6000 < Re < 10^6 \tag{25}$$

Where friction factor f is given by Eq. (26)

$$f = (1.82 \log Re - 1.64)^{-2} \tag{26}$$

The electrical efficiency of PV is expressed in terms of solar cell temperature, as shown in Eq. (27)

$$\eta_{electric} = 0.16(1 - 0.0045(T_{pv,s} - T_{ref})) \tag{27}$$

where T_{ref} is the reference temperature.

Fan power

In smooth ducts, the friction factor is calculated as shown in Eq. (28)-(30) (Incropera & DeWitt, 2001)

$$f = \frac{64}{Re} \qquad Re < 2300 \tag{28}$$

$$f = 0.316\, Re^{-1/4} \qquad 2300 < Re < 3000 \tag{29}$$

$$f = (0.790 \ln Re - 1.64)^{-2} \qquad 3000 < Re < 5 \times 10^6 \tag{30}$$

In the wire mesh packed duct, the friction factor is given by

$$f_p = 3.5722 \left(\frac{1}{nP}\right)^{1.0431} \left(\frac{p_t}{d_w}\right)^{1.1507} Re_p^{-0.43} \tag{31}$$

The relation between pressure drop and friction factor is

$$\Delta P = f \cdot \frac{L}{D_h} \cdot \frac{\rho V^2}{2} \tag{32}$$

For packed duct, the hydraulic radius r_h is used as the hydraulic diameter, and velocity is defined as $u = \frac{G_0}{\rho}$.

Thus, fan power can be calculated as

$$P_p = \frac{\dot{m} \Delta P}{\rho_f} \tag{33}$$

3 Results

Based on the above mathematical model, a computer program was developed to simulate the system. The results are presented in this section.

The effectiveness of different wire mesh in enhancing thermal performance of a solar air heater is first investigated. As listed in Table 2, two wire screen matrices are studied.

Table 2: Geometrical parameters of wire mesh matrices

Matrix number	Wire diameter $d_w(mm)$	Pitch $p_t(mm)$	No. of layers, n	Porosity, P	Hydralic radius, $r_h \times 10^3\ (m)$
A	1.06	2.16	5	0.82	1.2
B	1.22	2.54	9	0.63	0.52

The solar radiation of a winter noon in Montreal is used in the calculation. For the BIPV/T roof tilted at 30 degrees and the solar air heater tilted at 90 degrees, the radiation intensities are 527 W/m^2 and 600 W/m^2 respectively. The ambient air temperature in this study is set at 0 ºC. Air mass flow rate varies between 0.005 kg/s and 0.06 kg/s.

The thermal energy gains and fan power consumption of solar air heaters with and without wire screen matrices are compared in Figure 4. In general, the addition of wire mesh enhances the performance of solar air heater at low flow rates. As flow rate increases, the efficiency of packed solar air heater grows at a small rate, and its fan power consumption goes through considerable increase. It can also be seen that different packing matrix affects the performance of collector— the thermal energy gain is close, while mesh B consumes more fan power than mesh A. For this reason, in the following study, matrix A is used to evaluate the performance of the whole system.

By considering the outlet air temperature of the BIPV/T section as the inlet air temperature of the vertical solar air heater, the performance of the whole system can be evaluated. Figure 5 shows the thermal and electrical efficiencies for systems with and without wire screen matrices. The electrical efficiency of the packed system declined with increasing mass flow rate due to the fact that fan power increases significantly with rising flow rate for the packed bed. As expected, the thermal efficiency increase due to the wire mesh packed system is higher than that without packing, and the highest efficiency increase was about 9% when mass flow rate was 0.025 kg/s.

Figure 6 presents the outlet air temperature of the whole system with and without wire mesh packing. It can be seen that there is an increase of outlet temperature between 4ºC to 11ºC due to the wire mesh in mass flow rate range of 0.01 kg/s to 0.03 kg/s. According to Figure 4 and 5, the optimum mass flow rate is between 0.01 kg/s to 0.03 kg/s for the system with wire mesh, where energy efficiency is close to maximum and exit air temperature is around 4 °C to 11 ºC higher. The heat removal factor of the BIPV/T section is calculated for the optimum range, and is found to be 41.5% at 0.01 kg/s, 55.3% at 0.02 kg/s and 62.8% at 0.03kg/s.

The solar module temperature distribution changes with varying flow rate, which is depicted in Figure 7, resulting in higher electrical efficiency at higher flow rates due to the increased cooling effect.

Outlet air temperature is shown in terms of different solar radiation levels between 300 W/m^2 and 1000 W/m^2 in Figure 8. Outlet air temperature increases steadily with rising solar radiation.

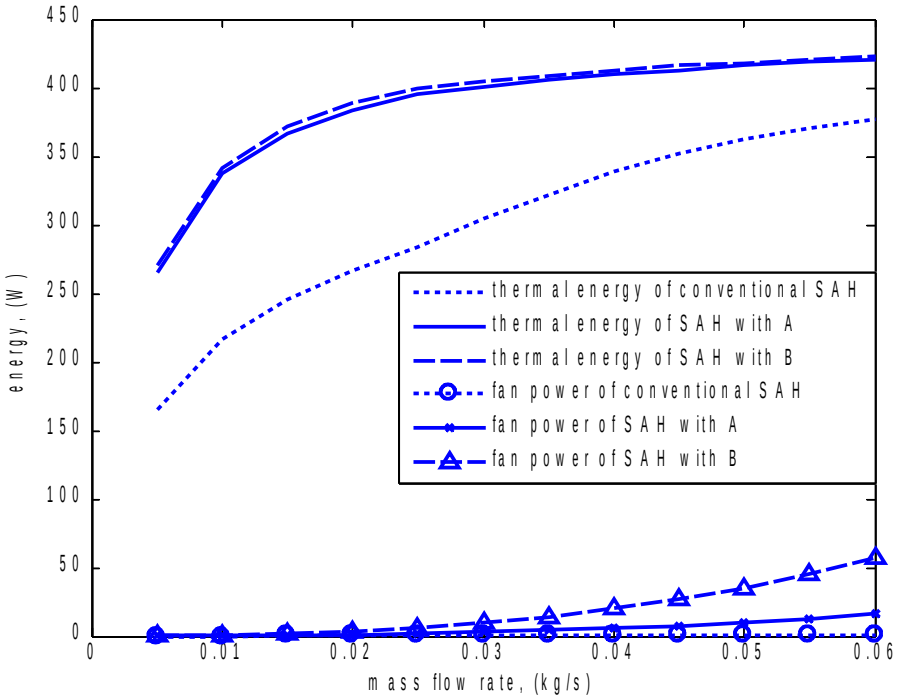

Figure 4: Comparison of thermal energy gain and fan power consumption between conventional solar air heater (SAH) versus SAH with different wire mesh packing (A or B – see Table 2)

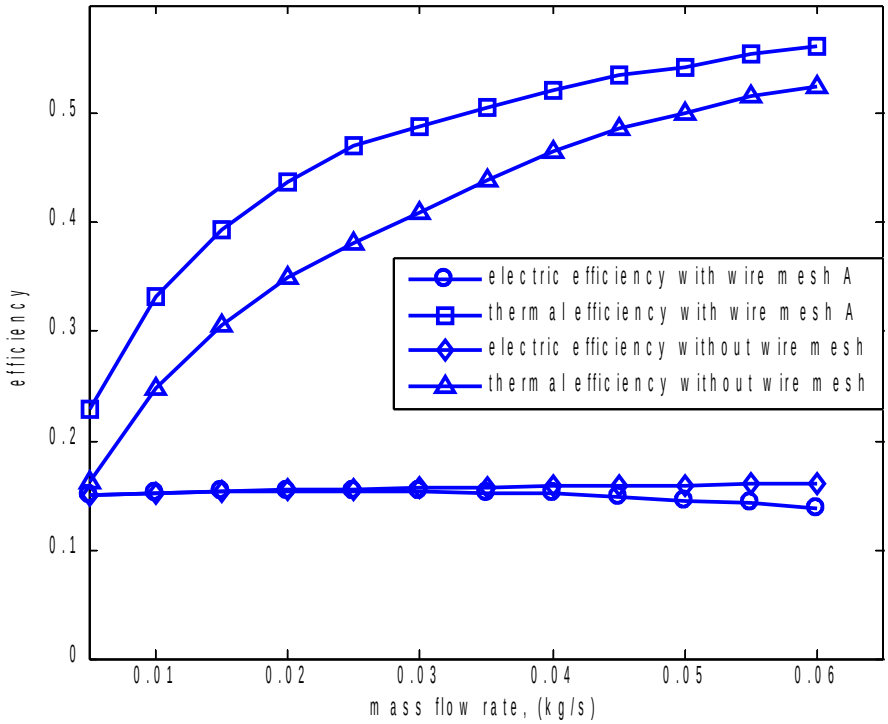

Figure 5: Electrical and thermal efficiencies of the whole BIPV/T system with and without wire mesh

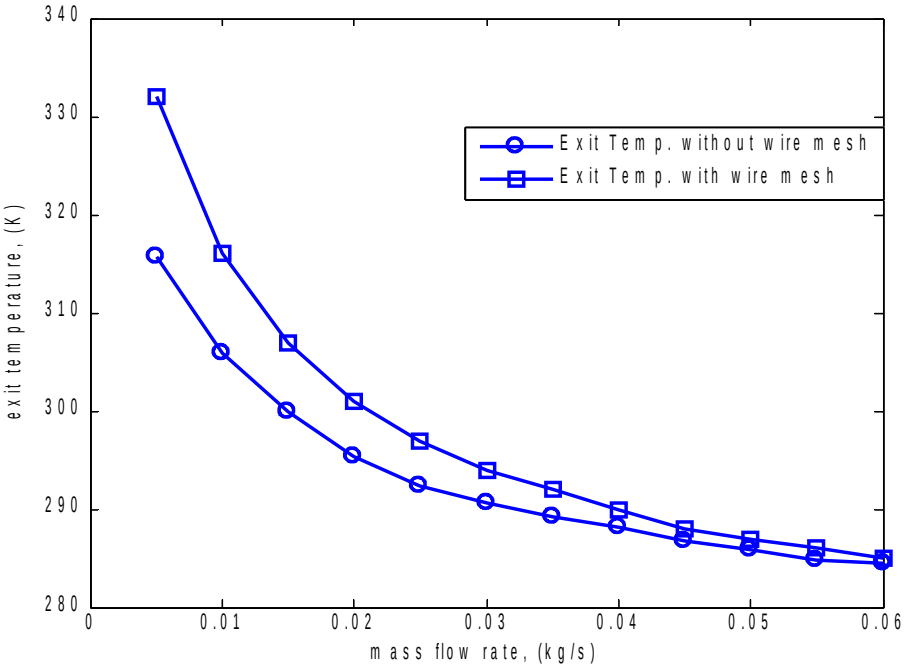

Figure 6: Exit air temperature of the whole BIPV/T system with and without wire mesh

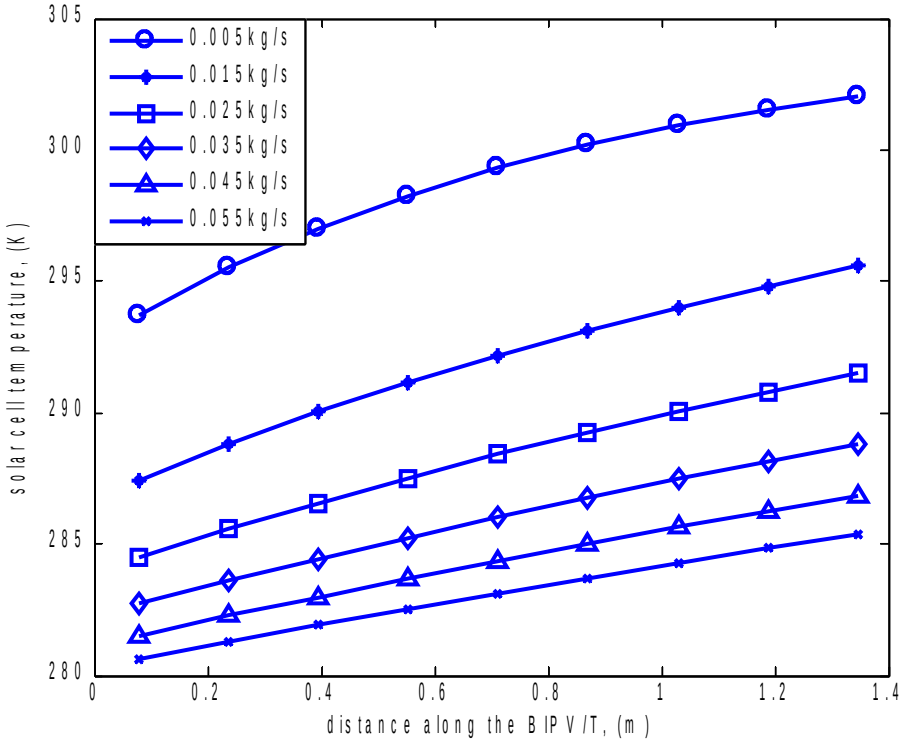

Figure 7: Solar module temperature distribution along the length of BIPV/T with changing mass flow rate

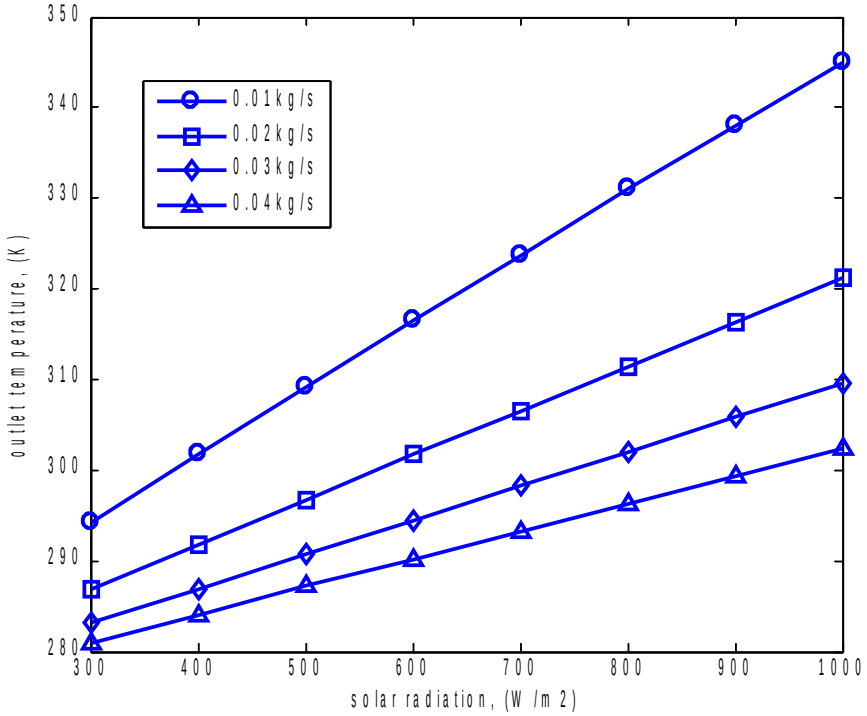

Figure 8: Outlet air temperature dependence on solar radiation level from 300 W/m^2 to 1000 W/m^2 (with ambient temperature of 0°C)

4 Conclusion

This paper presented a numerical study for an open loop air-based BIPV/T system with added glazed air collector section and wire mesh in order to obtain higher outlet air temperature for possible use with air source heat pumps in winter. The additional wire mesh packing in the vertical solar air heater has been shown to enhance its performance significantly. At mass flow rates lower than 0.03 kg/s, the enhancement is most significant. Wire mesh geometry had an important impact on system performance. In the present study, wire matrix A with a higher porosity and less layers has a positive effect on the whole BIPV/T system performance, which is most pronounced for flow rates between 0.01 kg/s and 0.03 kg/s. In this range, the thermal efficiency increased by 9% relative to that without wire mesh, and the outlet air temperature is also 4 °C to 11 °C higher than that without wire mesh for incident solar radiation equal to 600W/m^2. Simulations of yearly performance are underway and variations of PV and solar air collector lengths are being studied to generalize the results.

5 References

Agrawal, B., Tiwari, G.N., 2010, Optimizing the energy and exergy of building integrated photovoltaic thermal (BIPVT) systems under cold climate conditions, *Applied Energy*, 87, pp. 417-426.

Aldabbagh, B.Y.L., Egelioglu, F., Ilkan, M., 2010, Single and double pass solar air heaters with wire mesh as packing bed, *Energy*, 35, pp. 3783-3787.

Athienitis, K.A., Bambara, J., O'Neill B. & Faille J., 2011, A prototype photovoltaic/thermal system integrated with transpired collector, *Solar Energy*, 85, pp. 139-153.

Candanedo M.L., Athienitis, A., Park, K.W., 2011, Convective heat transfer coefficients in a building-integrated photovoltaic/thermal system, *Journal of Solar Energy Engineering*, 133.

Chen, Y.X., Athienitis, K.A., Galal, K., 2010, Modeling, design and thermal performance of a BIPV/T system thermally coupled with a ventilated concrete slab in a low energy solar house: Part 1, BIPV/T system and house energy concept, *Solar Energy*, 84, pp. 1892-1907.

Chow, T.T., Hand, J.W. & Strachan, P.A., 2003, Building-integrated photovoltaic and thermal applications in a subtropical hotel building, *Applied Thermal Engineering*, 23, pp. 2035-2049.

Chow, T.T., He W., Ji, J., & Chan, A.L.S., 2007, Performance evaluation of photovolta-ic-thermosyphon system for subtropical climate application, *Solar Energy*, 81, pp. 123-130.

Corbin, C.D. & Zhai Z.J., 2010, Experimental and numerical investigation on thermal and electrical performance of a building integrated photovoltaic-thermal collector system, *Energy and Buildings*,42, pp. 76-82.

Eicker, U., 2003, Solar Technologies for Buildings, John Wiley and Sons.

Fuentes, M.K., 1987, A simplified thermal model for flat-plate photovoltaic arrays, Sandia National Laboratories Report, SAND85-0330-UC-63, Albuquerque.

Huang, B.J., Lin, T.H., Hung, W.C., Sun, F.S., 2001, Performance evaluation of solar photovoltaic/thermal systems, *Solar Energy*, 70, pp. 443-448.

Incropera P.F., DeWitt, P.D., 2001, Fundamentals of heat and mass transfer, 5th edition, *John Wiley and Sons*.

Jiang, B., Ji, J., Yi, H., The influence of PV coverage ratio on thermal and electrical performance of photovoltaic-Trombe wall, *Renewable Energy*, 33, 2491-2498.

Omojaro, P.A., Aldabbagh, B.Y.L., 2010, Experimental performance of single and double pass solar air heater with fins and steel wire mesh as absorber, *Applied Energy*, 87, pp. 3759-3765.

Pantic, S., Candanedo, L., Athienitis, K.A., 2010, Modeling of energy performance of a house with three configurations of building-integrated photovoltaic/thermal system, *Energy and Buildings*, 42, pp. 1779-1789.

Prasad, B.S., Saini, S.J., Singh, M.K., 2009, Investigation of heat transfer and friciton characteristics of packed bed solar air heater using wire mesh as packing material, *Solar Energy*, 83, pp. 773-783.

Shahsavar, A., Salmanzadeh, M., Ameri, M. & Talebizadeh, P., 2011, Energy saving in buildings by using the exhaust and ventilation air for cooling of photovoltaic panels, *Energy and Buildings*, 43, pp. 2219-2226.

Thakur, S.N., Saini, S.J., Solanki, C.S., 2003, Heat transfer and friction factor correlations for packed bed solar air heater for a low porosity system, *Solar Energy*, 74, 319-329.

van Helden W.G.J., van Zolingen R.J.C., Zondag H.A., 2004, PV thermal systems: PV panels supplying renewable electricity and heat. *Progress in Photovoltaics: Research and Applications*, 12, pp. 415-426.

Varshney, L., Saini, S.J., 1998, Heat transfer and friction factor correlations for rectangular solar air heater duct packed with wire mesh screen matrices, *Solar Energy*, 62, pp. 255-262.

Watmuff, J.H., Charters, W.W.S., Proctor, D., 1977, Solar and wind induced external coefficients-Solar collectors, *Int. Revue d'Hellio-technique*, 2, p.56.